Ocean Modelling 000 (2015) 1–10

Contents lists available at ScienceDirect

Ocean Modelling

journal homepage: www.elsevier.com/locate/ocemod

Virtual Special Issue
Ocean Surface Waves

Statistical multi-model climate projections of surface ocean waves in Europe

Jorge Perez*, Melisa Menendez, Paula Camus, Fernando J. Mendez, Inigo J. Losada

Instituto de Hidráulica Ambiental "IH Cantabria", Universidad de Cantabria, Santander, Spain

ARTICLE INFO

Article history:
Received 8 February 2015
Revised 6 May 2015
Accepted 10 June 2015
Available online xxx

Keywords:
GCMs
Scenarios
Statistical downscaling
Wave climate
Weather types

ABSTRACT

In recent years, the impact of climate change on sea surface waves has received increasingly more attention by the climate community. Indeed, ocean waves reaching the coast play an important role in several processes concerning coastal communities, such as inundation and erosion. However, regional downscaling at the high spatial resolution necessary for coastal studies has received less attention. Here, we present a novel framework for regional wave climate projections and its application in the European region. Changes in the wave dynamics under different scenarios in the Northeast Atlantic Ocean and the Mediterranean are analyzed.

The multi-model projection methodology is based on a statistical downscaling approach. The statistical relation between the predictor (atmospheric conditions) and the predictand (multivariate wave climate) is based on a weather type (WT) classification. This atmospheric classification is developed by applying the k-means clustering technique over historical offshore sea level pressure (SLP) fields. Each WT is linked to sea wave conditions from a wave hindcast. This link is developed by associating atmospheric conditions from reanalysis with multivariate local waves. This predictor–predictand relationship is applied to the daily SLP fields from global climate models (GCMs) in order to project future changes in regional wave conditions. The GCMs used in the multi-model projection are selected according to skill criteria. The application of this framework uses CMIP5-based wave climate projections in Europe. The low computational requirements of the statistical approach allow a large number of GCMs and climate change scenarios to be studied.

Consistent with previous works on global wave climate projections, the estimated changes from the regional wave climate projections show a general decrease in wave heights and periods in the Atlantic Europe for the late twenty-first century. The regional projections, however, allow a more detailed spatial characterization of the projected changes under different climate scenarios. For example, changes in significant wave heights for the RCP8.5 scenario for the 2070–2099 time period indicate a general decrease of about 10 cm in Southern Europe (Portuguese, Spanish and French coasts) with respect to present conditions. This decrease is due to a higher occurrence of dominant and moderate Azores high pressure systems over the North Atlantic Ocean and a decrease in the persistence of intense low pressure systems at high latitudes.

1. Introduction

Reliable estimates of future wave climate parameters (i.e. significant wave height, mean wave period, mean wave direction) are essential for several applications such as coastal planning and design of coastal and offshore structures. Future wave climate is often estimated by extrapolating trends in historical data (e.g. Menendez et al., 2008). This approach, however, does not seem appropriate for the next century. Larger concentrations of greenhouse gases may lead to changes that are not captured in historical trends. In this context, global climate models (GCMs) have become valuable tools to estimate climate changes for different future climate scenarios. However, GCMs do not simulate ocean surface waves. Furthermore, the resolution of GCM-derived surface wind fields is often too coarse to force regional wave models.

There are two different approaches to generate regional wave climate projections. Dynamical downscaling, based on nesting of

* Corresponding author at: Instituto de Hidráulica Ambiental "IH Cantabria", Universidad de Cantabria, C/ Isabel Torres, 15, Parque Científico y Tecnológico de Cantabria, 39011 Santander, SPAIN. Tel.: +34 942 20 16 16x1217; fax: +34 942 26 63 61.
E-mail address: jorge.perezgarcia@unican.es (J. Perez).

http://dx.doi.org/10.1016/j.ocemod.2015.06.001
1463-5003/

numerical models, is perhaps the most widely used methodology (e.g. Erikson et al., 2015; Hemer et al., 2013a; Mori et al., 2010; Semedo et al., 2013). An alternative approach is statistical downscaling, which can be conducted, for example, by means of regression methods (e.g. Wang et al., 2014) or weather pattern-based approaches (e.g. Camus et al., 2014a). Laugel et al. (2014) showed that statistical projections can reproduce wave climatology as well as dynamical projections. Wang et al. (2010) found substantial similarity between both approaches in projected future changes. However, statistical methods were reported to perform better in reproducing the observed climate and interannual variability. Moreover, dynamical approaches are very computationaly expensive. Therefore, most dynamical wave climate projections studies are based on only one or a few GCMs (e.g. Laugel et al., 2014; Mori et al., 2010; Semedo et al., 2013). On the other hand, statistical approaches are much cheaper, thus, allowing the study of a large number of simulations. Analysis of multiple GCMs and climate scenarios is extremely important because cascading uncertainties can make outputs from two simulations very different. Furthermore, a large ensemble gives more robust projections and a measure of uncertainties (Gleckler et al., 2008).

In this work, a weather type (WT) statistical downscaling for multivariate ocean wave climate is presented. This method is based on a statistical downscaling framework able to reproduce the seasonal and interannual variability of wave climate (Camus et al., 2014a) and takes into account the skill of GCMs to define an optimal ensemble of models (Perez et al., 2014a). Application of this method is demonstrated through wave climate projections in the European region with a spatial resolution up to 0.125° (less than 15 km along the coast).

The paper is presented in five sections. Following the introduction, Section 2 presents the databases (reanalysis, wave hindcast and GCMs) used in this study. Section 3 explains the methodology that has been developed, describing the WT classification, the downscaling technique, and the selection of the ensemble of GCMs. The study is completed with presentation of the results in Section 4 and the conclusions in Section 5.

2. Data

2.1. Historical atmospheric data

Reanalyses are designed to provide global gridded representations of the atmosphere–ocean–land surface–sea ice system over a long historical period of time. The National Centers for Environmental Prediction (NCEP) Climate Forecast System Reanalysis (CFSR, Saha et al., 2010) is a reanalysis dataset that represents an improvement in the field due to its high resolution and advanced data-assimilation techniques. Beginning in 2011, CFSR is extended by NCEP's Climate Forecast System Version 2 (CFSv2, Saha et al., 2014) operational model. We use near-surface winds, ice coverage, and sea level pressure fields from CFSR and CFSv2. CFSR and CFSv2 outputs are available at an hourly time resolution from 1979 onward. Global winds and ice coverage at a horizontal resolution of ~0.3° (~0.2° for CFSv2) were used as forcing for a wave hindcast. SLP fields at a 0.5° horizontal resolution were used to create a WT classification.

2.2. Historical wave data

In this study, we have conducted a wave hindcast from 1979 to 2013 with hourly resolution to provide historical wave data. This hindcast uses WaveWatch III wave model (version 4.18, Tolman, 2014) in a multigrid configuration. The multigrid is composed of several regular grids with two-way nesting: a global grid (1° latitude × 1.5° longitude), a grid covering the Atlantic Ocean (0.5° × 0.5°) and a grid in the area close to the European coastline (0.125° × 0.125°). Small grids covering the archipelagos of Cape Verde, Canary Islands and Azores (0.125° × 0.125°) are also used to improve the modeling of wave shadowing effects. Winds and ice coverage were interpolated from CFSR and CFSv2 data. The bathymetry, land-sea mask, and obstruction grids for unresolved boundaries for each grid were obtained using the automated generation software for WaveWatch III (Chawla and Tolman, 2008). We used this software with etopo1 bathymetry (Amante and Eakins, 2009) and coastlines from the global self-consistent, hierarchical, high-resolution geography database (GSHHG, Wessel and Smith, 1996).

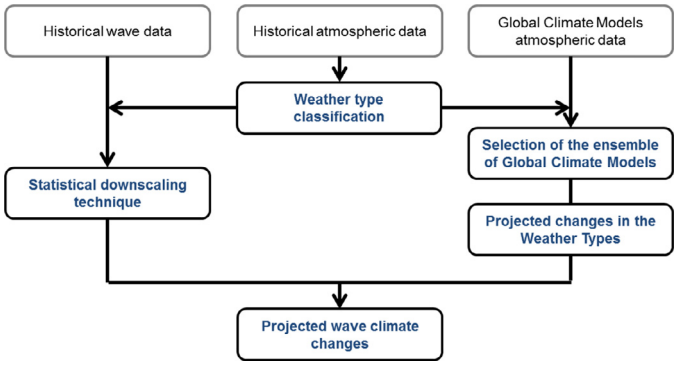

Fig. 1. Flowchart representing the methodology to obtain wave climate projections.

Wave spectra in WaveWatch III were defined by 32 frequencies ranging non-linearly from 0.0372 Hz to 0.714 Hz with a factor of 1.1 and 24 direction bins. WaveWatch III was implemented using the parameterization TEST451 (Ardhuin et al., 2010) because the wave heights obtained with TEST451 (e.g. Rascle and Arhuin, 2013) have smaller biases than those obtained with older parameterizations. Validation against buoys and altimeter data (not shown) confirmed a good agreement of this hindcast with observations. For example, the comparison between altimeter measured and modeled significant wave heights on the European grid shows a 0.95 correlation and a scatter index of less than 0.2. The best agreement is found in the Atlantic Ocean while the worst agreement is found in some semi-enclosed basins such as the Alboran Sea and the Adriatic Sea.

2.3. Global climate models atmospheric data

We analyzed daily SLP fields from CMIP5 GCMs to study changes in atmospheric circulation. Data from historical experiments from 1975 to 2004 was used to characterize recent past conditions. Data from representative concentration pathways (RCPs, Moss et al., 2010) from 2010 to 2100 were used to represent future conditions. These time periods were chosen because they overlap with data available from most GCMs. The three selected RCPs included one mitigation scenario leading to a very low forcing level (RCP2.6), one medium stabilization scenario (RCP4.5) and one very high baseline emission scenario (RCP8.5) leading to high greenhouse concentration levels (van Vuuren et al., 2011). All the simulations available (at the time this work was conducted) for these scenarios were analyzed. This resulted in a total of 42 GCMs with 137 historical simulations, 56 RCP2.6 simulations, 98 RCP4.5 simulations and 72 RCP8.5 simulations. The CMIP5 data used in this study were obtained via the Earth System Grid-Center for Enabling Technologies (ESG-CET, http://pcmdi9.llnl.gov/).

3. Methods

3.1. Framework

Fig. 1 summarizes the methodology to obtain regional wave climate projections. This methodology requires three sources of data: historical wave data, historical atmospheric data and GCM simulated atmospheric data. First, an automated WT classification is performed using the historical atmospheric data from a reanalysis. This

Please cite this article as: J. Perez et al., Statistical multi-model climate projections of surface ocean waves in Europe, Ocean Modelling (2015), http://dx.doi.org/10.1016/j.ocemod.2015.06.001

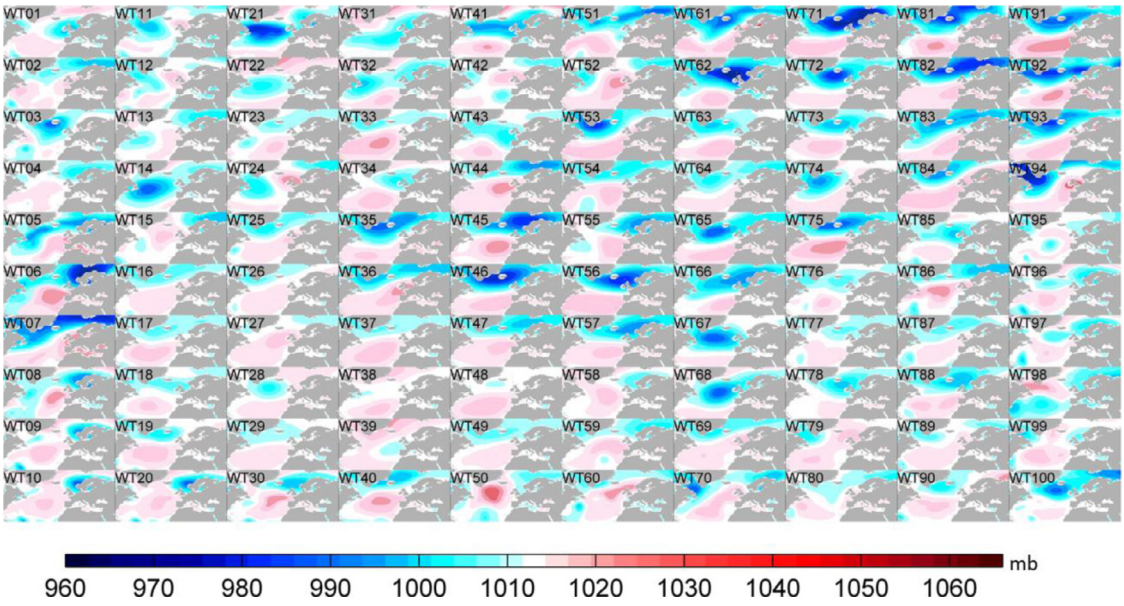

Fig. 2. The 100 weather types represented by the 3-day averaged SLP fields (mb).

Table 1
Evaluation of the performance of the CMIP5 GCMs. Selected GCMs in bold.

Number	Model Thresholds	SI 0.86	RE 0.36	stdSI 0.50	SI_{DJF} 1.03	SI_{MAM} 1.10	SI_{JJA} 2.78	SI_{SON} 1.09	Consist. Q1−1.5IQR Q3+1.5IQR
01	**CMCC-CMS**	**0.39**	**0.20**	**0.36**	**0.79**	**0.81**	**0.83**	**0.51**	**V**
02	**MPI-ESM-LR**	**0.42**	**0.19**	**0.39**	**0.73**	**0.84**	**1.50**	**0.63**	**V**
03(OUT)	MPI-ESM-P	0.42	0.18	0.39	0.68	0.72	1.53	0.68	(OUT)
04	**ACCESS1.3**	**0.42**	**0.21**	**0.42**	**0.76**	**0.87**	**1.21**	**0.68**	**V**
05	**EC-EARTH**	**0.44**	**0.19**	**0.41**	**0.67**	**0.89**	**1.19**	**0.69**	**V**
06	**CMCC-CM**	**0.45**	**0.23**	**0.37**	**0.74**	**0.85**	**1.37**	**0.60**	**V**
07	**MPI-ESM-MR**	**0.46**	**0.20**	**0.38**	**0.60**	**0.81**	**1.73**	**0.55**	**V**
08	**HadGEM2-CC**	**0.48**	**0.21**	**0.40**	**0.60**	**0.68**	**1.35**	**0.94**	**V**
09	**ACCESS1.0**	**0.49**	**0.22**	**0.41**	**0.67**	**0.62**	**1.61**	**0.92**	**V**
10(OUT)	HadGEM2-AO	0.51	0.22	0.48	0.58	0.72	1.50	1.11(OUT)	(OUT)
11	**CNRM-CM5**	**0.52**	**0.23**	**0.42**	**0.72**	**0.81**	**1.42**	**0.94**	**V**
12(OUT)	GISS-E2-H	0.53	0.24	0.43	0.92	0.84	1.68	0.65	(OUT)
13	**HadGEM2-ES**	**0.53**	**0.22**	**0.42**	**0.61**	**0.74**	**1.61**	**0.94**	**V**
14(OUT)	CESM1(CAM5)	0.55	0.25	0.47	0.71	0.73	1.30	0.98	(OUT)
15(OUT)	NorESM1-M	0.56	0.27	0.42	0.85	1.18(OUT)	1.62	0.86	(OUT)
16(OUT)	CMCC-CESM	0.58	0.28	0.48	0.99	1.16(OUT)	1.20	0.92	V
17(OUT)	MIROC-ESM-CHEM	0.58	0.30	0.50(OUT)	0.96	1.20(OUT)	1.80	1.08	(OUT)
18(OUT)	BCC-CSM1.1	0.59	0.26	0.42	0.92	1.06	2.06	0.72	(OUT)
19(OUT)	GFDL-ESM2M	0.61	0.26	0.41	0.79	0.80	1.78	0.95	(OUT)
20	**GISS-E2-R**	**0.62**	**0.27**	**0.43**	**0.90**	**0.92**	**2.32**	**0.68**	**V**
21	**BNU-ESM**	**0.65**	**0.29**	**0.44**	**1.01**	**0.97**	**1.73**	**1.04**	**V**
22(OUT)	FGOALS-g2	0.65	0.32	0.44	1.00	0.99	1.43	0.70	(OUT)
23	**HadCM3**	**0.65**	**0.28**	**0.44**	**0.99**	**1.06**	**1.38**	**0.67**	**V**
24	**CanESM2**	**0.67**	**0.32**	**0.48**	**0.93**	**0.89**	**1.71**	**1.05**	**V**
25(OUT)	MIROC-ESM	0.71	0.33	0.50(OUT)	1.00	1.06	2.32	0.90	V
26	**MIROC4h**	**0.71**	**0.31**	**0.41**	**0.95**	**0.74**	**1.56**	**0.97**	**V**
27(OUT)	CCSM4	0.73	0.35	0.47	1.07(OUT)	1.08	2.21	0.91	V
28(OUT)	BCC-CSM1.1(m)	0.76	0.32	0.47	1.11(OUT)	1.23(OUT)	2.28	1.01	V
29	**GFDL-ESM2G**	**0.77**	**0.28**	**0.42**	**0.76**	**0.79**	**2.39**	**1.02**	**V**
30(OUT)	IPSL-CM5A-MR	0.78	0.35	0.52(OUT)	0.85	1.14(OUT)	2.55	1.09(OUT)	V
31	**CanCM4**	**0.78**	**0.34**	**0.47**	**0.97**	**0.96**	**2.26**	**1.08**	**V**
32(OUT)	CESM1(BGC)	0.80	0.37(OUT)	0.49	1.15(OUT)	0.92	2.36	0.95	V
33(OUT)	CESM1(FASTCHEM)	0.83	0.36(OUT)	0.52(OUT)	1.01	1.10	2.71	0.89	V
34(OUT)	GFDL-CM3	0.84	0.31	0.44	0.68	0.84	3.01(OUT)	0.80	(OUT)
35(OUT)	INM-CM4	0.88(OUT)	0.31	0.44	0.84	1.04	3.36(OUT)	0.82	V
36(OUT)	IPSL-CM5B-LR	0.89(OUT)	0.35	0.47	0.67	0.93	3.52(OUT)	0.68	V
37(OUT)	IPSL-CM5A-LR	0.92(OUT)	0.39(OUT)	0.54(OUT)	0.88	1.03	3.16(OUT)	1.11(OUT)	(OUT)
38(OUT)	MIROC5	0.93(OUT)	0.32	0.41	0.92	0.93	2.52	1.04	V
39(OUT)	FGOALS-s2	0.95(OUT)	0.43(OUT)	0.58(OUT)	1.28(OUT)	1.00	2.78(OUT)	1.29(OUT)	(OUT)
40(OUT)	CSIRO-Mk3.6.0	0.98(OUT)	0.39(OUT)	0.49	1.24(OUT)	1.13(OUT)	2.80(OUT)	1.13(OUT)	V
41(OUT)	MRI-CGCM3	1.03(OUT)	0.40(OUT)	0.48	0.83	1.11(OUT)	3.42(OUT)	1.23(OUT)	(OUT)
42(OUT)	MRI-ESM1	1.08(OUT)	0.42(OUT)	0.50(OUT)	0.79	1.15(OUT)	3.78(OUT)	1.09(OUT)	V

Please cite this article as: J. Perez et al., Statistical multi-model climate projections of surface ocean waves in Europe, Ocean Modelling (2015), http://dx.doi.org/10.1016/j.ocemod.2015.06.001

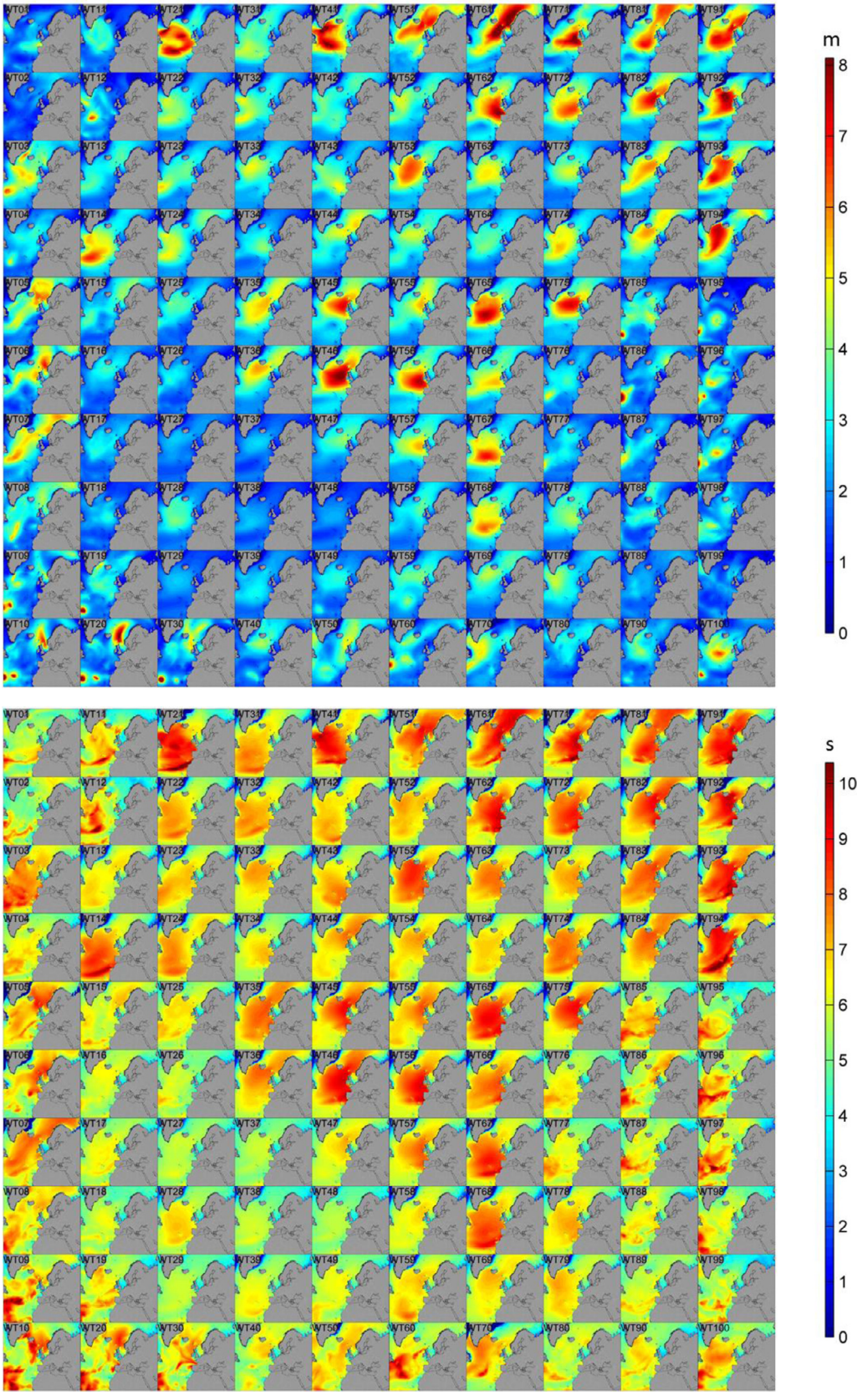

Fig. 3. H_s, in meters (top) and T_{02}, in seconds (bottom) associated to each weather type.

Please cite this article as: J. Perez et al., Statistical multi-model climate projections of surface ocean waves in Europe, Ocean Modelling (2015), http://dx.doi.org/10.1016/j.ocemod.2015.06.001

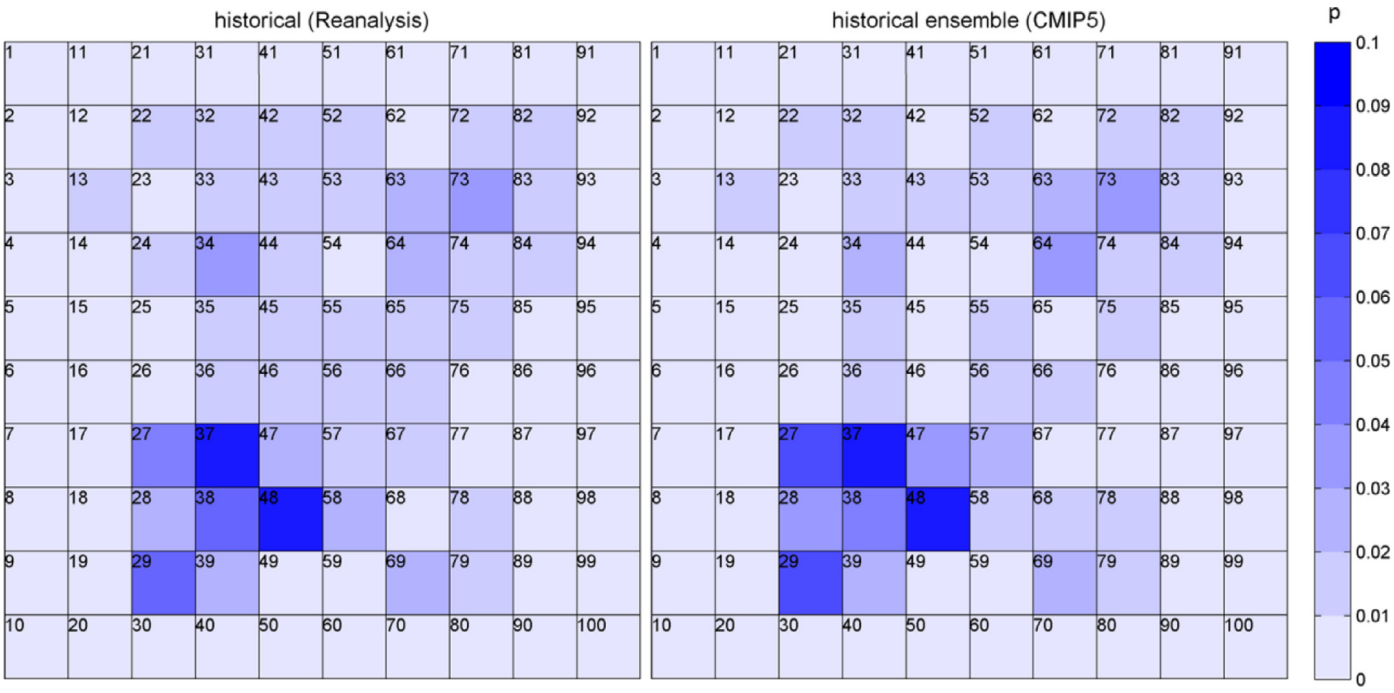

Fig. 4. Relative frequencies of weather types during the control period (1979–2004) for reanalysis (left) and the ensemble of GCMs (right).

classification is used for two purposes: (1) Each WT is linked to corresponding historical wave conditions from a wave hindcast in order to obtain an empirical statistical relationship between atmospheric circulation and wave climate. (2) Historical and future frequencies of each WT are analyzed to select the best ensemble of GCMs and project the changes in the frequency of the WTs for this ensemble. Finally, wave climate projections are obtained by applying the statistical relationship between atmospheric conditions and wave climate to the atmospheric data from GCMs.

3.2. Weather type classification

There are several methodologies to make a classification of WTs. A classification can be subjective (e.g. Lamb, 1972) or based on automated algorithms such as neural networks or clustering. In this work, an automated WT classification is applied. The WT classification is based on two main steps: the definition of the predictor and the clustering technique.

The predictor is constructed with the SLP fields from CFSR and CFSv2 during the period from 1979 to 2013. The spatial and time resolutions of GCMs are too coarse to allow a direct comparison with the atmospheric reanalysis. Therefore, daily SLP fields from the hourly reanalysis data were regridded to a $1° \times 1°$ lattice. Swell energy in ocean basins propagate for thousands of kilometers over several days (e.g. Snodgrass et al., 1966). Accordingly, the atmospheric conditions during the time of propagation of the waves have to be taken into account (Camus et al., 2014b). Consequently, the predictor representing one day is composed of the averaged SLP and squared SLP gradients over that day and the previous two days. The squared SLP gradients, related to geostrophic winds, are included because they have been shown to provide a good predictor of ocean waves (Wang et al., 2014). The spatial limits of the predictor must include the area where the most important wave generation/dissipation processes occur. ESTELA (Perez et al., 2014b) is a technique for evaluating the origin and travel times of the wave energy reaching a local area. Given that the goal of this work is to characterize regional wave climate projections in Europe, we have checked over the ESTELA maps for locations further north, west, east and southern European coasts to select an area from 20°N to 80°N and from 60°W to 50°E. Summarizing, the predictor for a specific day is the 3-day average of both SLP and squared SLP gradients in all the ocean points of the selected area.

The clustering technique is described in Camus et al. (2014a) and is based on three steps: First, a principal component analysis (PCA) is applied to the predictor in order to reduce the data dimensionality. PCA finds a new optimal basis for the data (Preisendorfer, 1988). The projected data in this new basis (principal components, PCs) is sorted in an increasing order of explained variance. Therefore, the data dimensionality is reduced by keeping only the PCs that explains the 95% of the variance. Second, the predictor in the empirical orthogonal function (EOF) space is clustered using the k-means algorithm. Daily predictors are grouped into N clusters that minimize the overall within-cluster distance. Each cluster is formed by the most similar predictor fields and represented by a centroid defined as the mean of these fields. Finally, the WTs are arranged in a lattice that minimizes the differences between contiguous WTs.

Daily predictor fields are grouped in certain atmospheric circulation patterns. The main goal of this classification is to correctly represent the empirical relationship between atmospheric circulation and wave climate along the European coasts. This objective requires a large number of atmospheric circulation patterns because similar WTs can generate vastly different wave conditions at specific locations, especially in areas affected by a complex bathymetry and coastline. After preliminary tests, we have determined that $N = 100$ WTs fulfils the compromise between a significant number of WTs and a minimum number of data per group. Wave climate projections are not overly sensitive to small differences in the number of WTs, though, a smaller number of WTs is not enough to estimate both the spatial patterns and its intensities, and a larger number of WTs may result in some WTs with no data. Fig. 2 shows the 100 WTs, represented by the 3-day averaged SLP fields, organized in a bidimensional lattice. The clustering method identifies different low pressure systems. Low pressure centers located at the north polar region can be found in the upper right corner of the lattice (e.g. WTs 51, 61, 71). Low pressure centers located southward are characterized by patterns in the middle of the lattice (e.g. WTs 46, 56, 57). The mildest synoptic patterns are located around the WT 38.

Please cite this article as: J. Perez et al., Statistical multi-model climate projections of surface ocean waves in Europe, Ocean Modelling (2015), http://dx.doi.org/10.1016/j.ocemod.2015.06.001

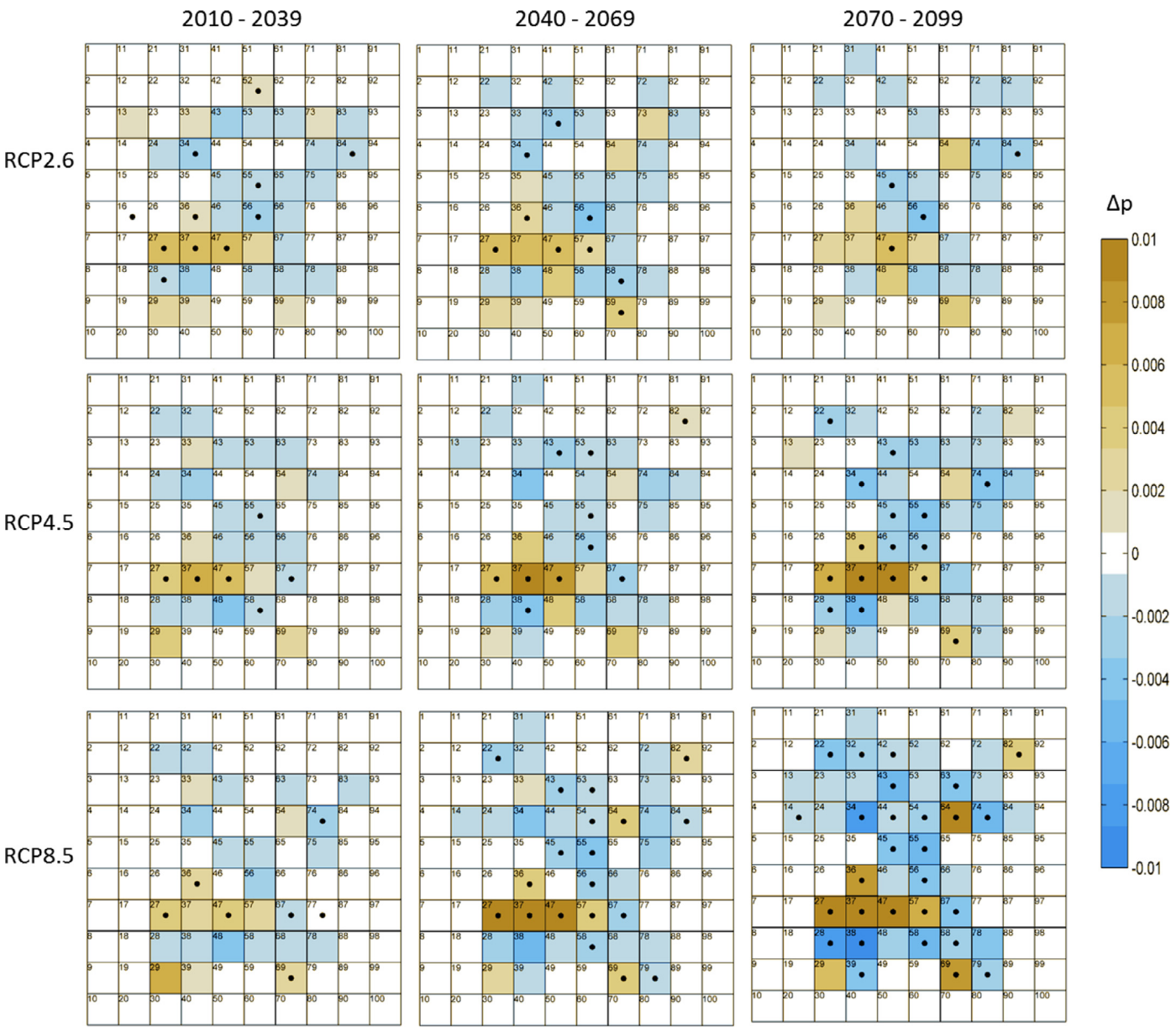

Fig. 5. Changes in the frequency of the weather types for different scenarios (rcp2.6 up, rcp4.5 middle and rcp8.5 down) and time periods (2010–2039 left, 2040–2069 middle and 2070–2099 right) towards the reference period (1975–2004). Dots in the weather types indicate agreement on the sign of change of more than 80% of the models.

3.3. Statistical downscaling technique

The WT classification described in the previous section can be used to link the atmospheric conditions (predictor) to the wave climate (predictand). In this work, every WT is linked to the multivariate wave climate during the wave hindcast (1979–2013). The link is derived by associating the hourly sea-state, i.e. wave parameters such as the significant wave height (H_s) and the second-order spectral mean period (T_{02}), with the WT at the same day. The probability distribution of a certain sea state parameter for each WT is defined associating the hourly sea states to the daily predictor fields corresponding to that WT. The total probability distribution is defined as the sum of the distribution multiplied by the probability of occurrence of each WT. A detailed description of this procedure and validation analysis at two locations in the Irish and the Spanish coasts is presented in Camus et al. (2014a).

Fig. 3 shows mean H_s and mean T_{02} in the North Atlantic associated with each WT. Comparing Figs. 2 and 3, the predictor–predictand relationship can be clearly understood. The position of the low pressure centers are reflected in the spatial pattern of H_s and T_{02}. For example, energetic waves along the Norwegian and England coasts are generated for WTs 51, 61 and 71, while the highest waves along the French and Spanish coasts are associated with WTs 46 and 56. The effect of the different low pressure patterns can also be detected in the mean wave period field. Notably, deeper lows are associated with larger wave periods as well as larger wave heights.

The relationship between predictor and predictand can be extrapolated to the future if we assume the hypothesis of stationary, that is, the relative frequencies of the WTs can vary over time but the predictor–predictand relationship remains constant. With this assumption, the distribution $f(y)$ of different variables (e.g. H_s) in a new time period can be obtained as follows:

$$f(y) = \sum_{i=1}^{N} p_i f_i(y), \quad (1)$$

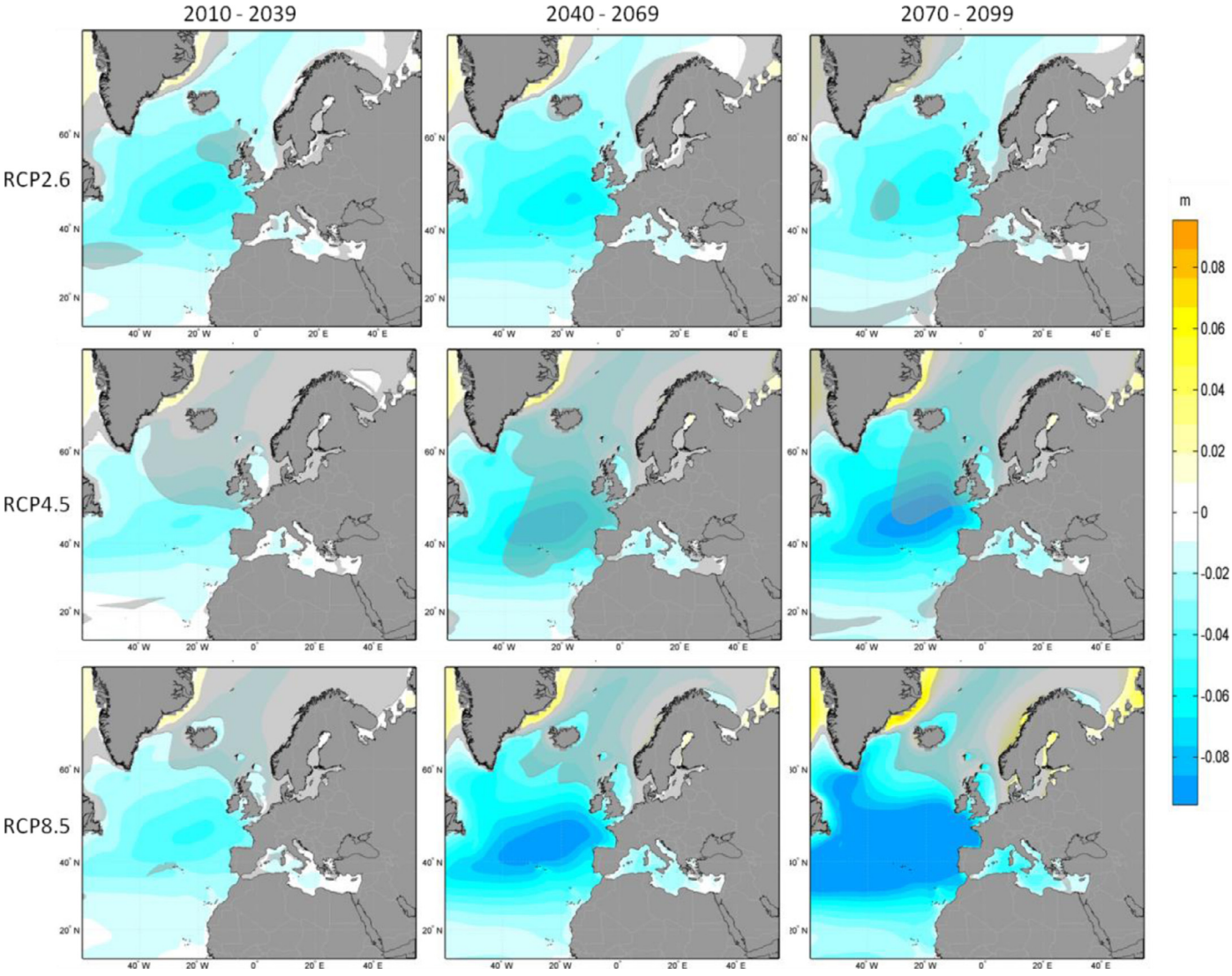

Fig. 6. Changes in mean significant wave heights in the Eastern North Atlantic, in meters, for different scenarios (rcp2.6 top, rcp4.5 middle, and rcp8.5 bottom) and time periods (2010–2039 left, 2040–2069 middle, and 2070–2099 right) towards the reference period (1975–2004). No shadowed areas indicate agreement on the sign of change of more than 80% of the models.

where p_i is the relative frequency of the ith WT during the new period, $f_i(y)$ is the conditional distribution of the predictand for the ith WT and N is the number of WTs. The new frequencies (p_i) are computed by assigning each atmospheric situation to the most similar WT in the EOF space.

3.4. Selection of the ensemble of global climate models

The historical and future simulations from the CMIP5 GCMs are projected on the WT classification and their climatology is evaluated. The projection is made after regridding each model's output to a common $1° \times 1°$ grid. We have followed the methodology and performance indices proposed by Perez et al. (2014a) to analyze the reliability of different GCMs. In this methodology three factors are analyzed: (1) the skill of GCMs to reproduce historical synoptic situations, (2) the skill of GCMs to reproduce the historical climate variability (interannual and seasonal), and (3) the consistency of GCMs in twenty-first century projections.

Results of this analysis are summarized in Table 1. In order to examine a wide range of processes we study eight different indices: SI, RE, stdSI, SI_{DJF}, SI_{MAM}, SI_{JJA}, SI_{SON} and consistency. When multiple simulations are available, the mean value of the index is considered. The skill to reproduce historical synoptic situations and climate variability are studied by comparing the GCMs to CFSR during the control period from 1979 to 2004. This period is chosen because CFSR begins in 1979 and most historical GCM simulations end in 2005. The first two indices measure the skill of the GCMs to reproduce historical synoptic situations from CFSR. SI is the root mean square error normalized by the mean frequency, and RE is a log-Euclidean distance. SI and RE measure absolute and relative differences in frequencies of the WTs, respectively. The next five indices measure the ability to reproduce the climate variability in CFSR. StdSI analyzes the interannual variability and the four seasonal metrics (SI_{DJF}, SI_{MAM}, SI_{JJA}, SI_{SON}) analyze the climatology within the four seasons. The last index (consistency) analyzes changes in the climatology and interannual variability in order to detect GCMs with inconsistent future simulations, i.e., with a behavior vastly different than those of most GCMs. The consistency index analyzes the magnitude of changes between the historical experiment for the reference period (1975–2004) and the RCPs for three periods of thirty years during the twenty-first century (2010–2039, 2040–2069 and 2070–2099).

Given the variability among GCMs, we use the results of the evaluation of the GCMs to generate a reduced ensemble. We defined thresholds for the eight studied indices. GCMs over any of those

Please cite this article as: J. Perez et al., Statistical multi-model climate projections of surface ocean waves in Europe, Ocean Modelling (2015), http://dx.doi.org/10.1016/j.ocemod.2015.06.001

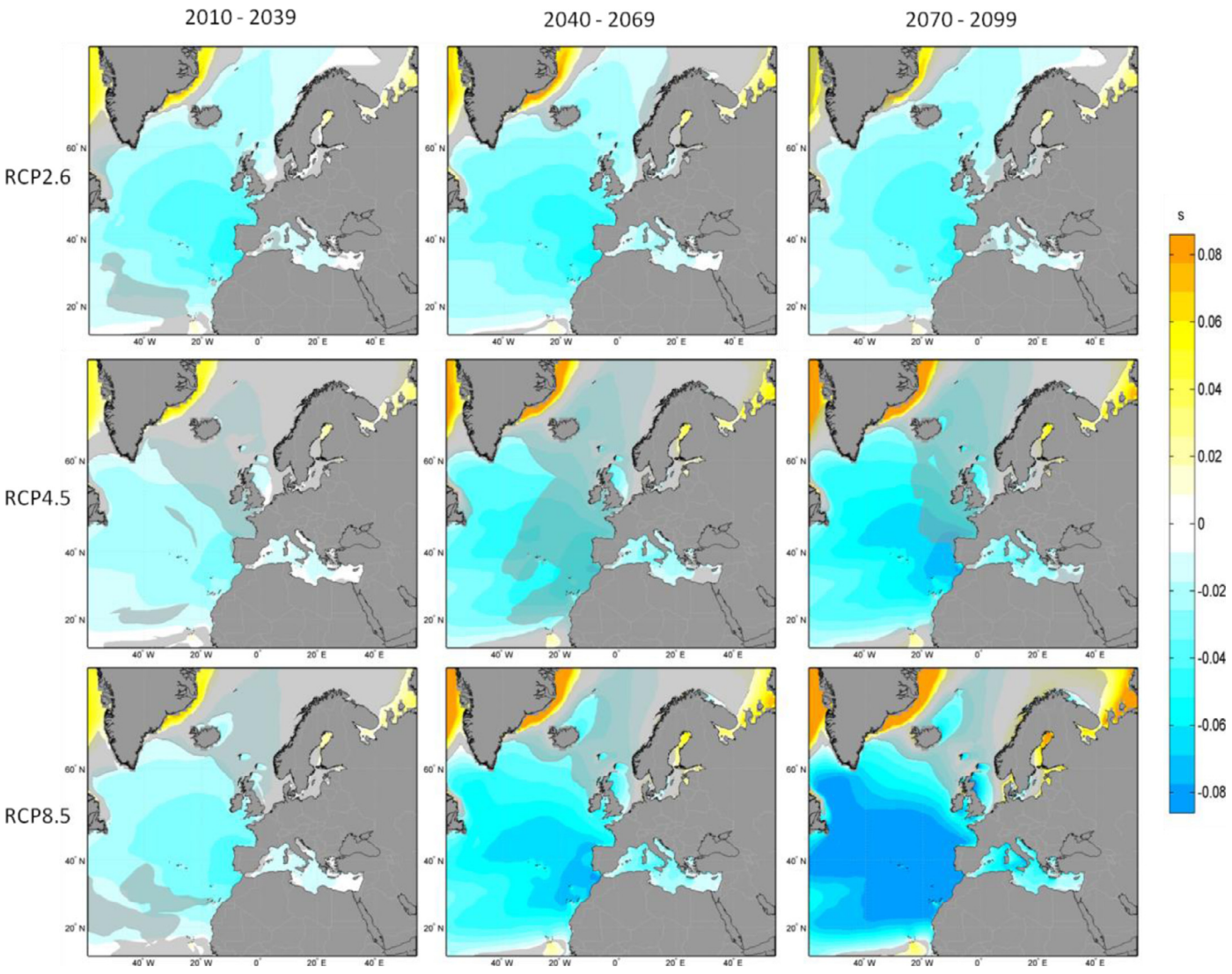

Fig. 7. Changes in mean T_{02} wave periods in the Eastern North Atlantic, in seconds, for different scenarios (rcp2.6 top, rcp4.5 middle, and rcp8.5 bottom) and time periods (2010–2039 left, 2040–2069 middle, and 2070–2099 right) towards the reference period (1975–2004). No shadowed areas indicate agreement on the sign of change of more than 80% of the models.

thresholds are excluded from the reduced ensemble. The thresholds selected for all indices (except consistency) are the mean value of the index plus one standard deviation. For consistency, we consider two thresholds, the first quartile minus 1.5 times the interquartile range (IQR) and the third quartile plus 1.5 IQR. The ensemble is generated by simply averaging the relative frequencies of the individual GCMs. The reduced ensemble obtained using these thresholds is composed of 17 of the initial 42 models. This ensemble provides results with good agreement with historical climatology and high consistency. Therefore, it is reasonable to assume that future predictions based on this ensemble would be more reliable than those produced from a single GCM or an unfiltered ensemble. It is important to note, however, that the ensemble could be specified differently according to specific needs. For example, using all the available GCMs may give a better measure of the inter-model variability. Relative frequencies during the control period for CFSR and the reduced ensemble of GCMs are shown in Fig. 4. Frequencies obtained from these two sources of data are very similar, but minor differences can be found. For example, the frequencies of WTs 44, 45, 46 and 65, associated with large swells, are underestimated by the GCM ensemble.

4. Results

4.1. Projected changes in the weather types

The WT classification of CFSR has been used to analyze the historical atmospheric circulation over Europe and predict changes to it. Projected changes in the relative frequency of the WTs during twenty-first century are computed for several scenarios using data from GCMs. We have analyzed three future scenarios (RCP2.6, RCP4.5 and RCP8.5) in three future periods (2010–2039, 2040–2069 and 2070–2099) against the reference period (1975–2004). We compare each simulation against its own representation of the reference period when analyzing changes. Fig. 5 shows patterns of change of the ensemble with respect to the reference period for different scenarios and time periods. The pattern of the changes is fairly consistent across scenarios and periods. However, high emissions scenarios lead to more intense changes than those of low emissions scenarios, and long-term changes are larger than short-term changes. An increase in frequencies of a group of WTs in the bottom left part of the classification (e.g. 27, 36, 37, 47 and 57) is noticeable. These WTs correspond to situations with gentle SLP gradients and small waves. A decrease in frequency of WTs associate with large waves (e.g. 45, 46, 55 and 56)

Please cite this article as: J. Perez et al., Statistical multi-model climate projections of surface ocean waves in Europe, Ocean Modelling (2015), http://dx.doi.org/10.1016/j.ocemod.2015.06.001

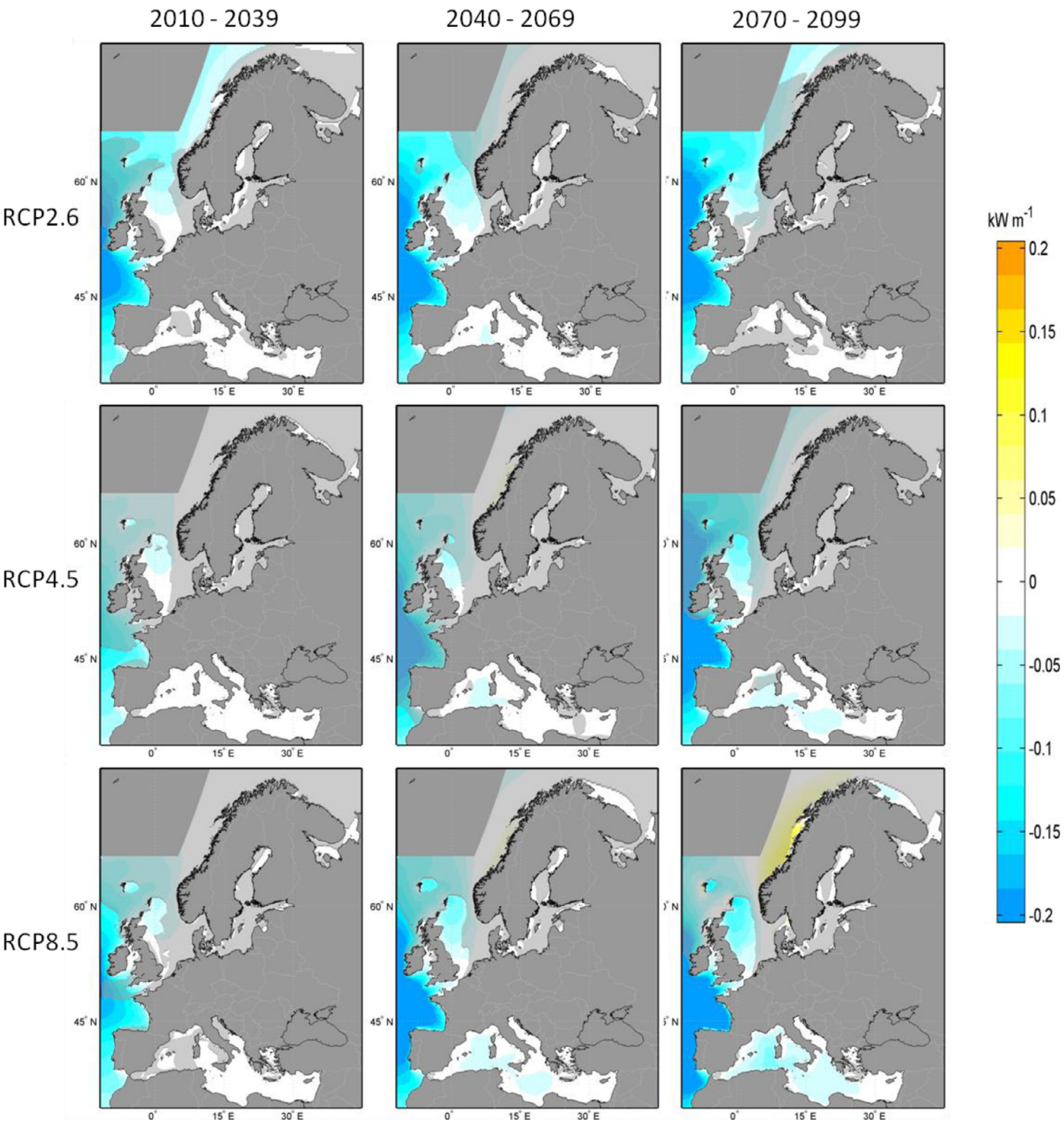

Fig. 8. Changes in mean energy flux along the European coastline, in kWm^{-1}, for different scenarios (rcp2.6 top, rcp4.5 middle, and rcp8.5 bottom) and time periods (2010–2039 left, 2040–2069 middle, and 2070–2099 right) towards the reference period (1975–2004). No shadowed areas indicate agreement on the sign of change of more than 80% of the models.

can also be seen. As a result of these changes in the WT frequency, an intensification of the Azores high and a decrease of the Iceland low pressure system are expected. These changes agree with the ensemble mean of projected changes in SLP reported by Wang et al. (2014).

4.2. Projected wave climate changes

The statistical downscaling technique is applied to the WT frequencies from GCMs to obtain changes in wave climate. Changes in the short- (2010–2039), mid- (2040–2069) and long-term (2070–2099) are computed with respect to the reference period (1975–2004). Fig. 6 shows projected changes in the mean H_s in the North Atlantic on a grid of 0.5°. A decrease in H_s can be seen in all areas except in the north, where small increases can be found. The increase in the Norwegian coasts is mainly produced by the intensification of WT82. The increases off the coasts of Greenland and Russia should be analyzed carefully because they are found in areas often covered by ice, and may be associated with changes in the ice coverage. The

Please cite this article as: J. Perez et al., Statistical multi-model climate projections of surface ocean waves in Europe, Ocean Modelling (2015), http://dx.doi.org/10.1016/j.ocemod.2015.06.001

behavior for all scenarios is similar in the short-term with small reductions in wave height, but differs in the mid- and long-term. In the long-term, especialy for RCP8.5, decreases in wave heights are much larger, reaching values of 10 cm in latitudes around 40°N. These results are consistent with previous studies of Hemer et al. (2013b), Wang et al. (2014) and Mori et al. (2010), though, Wang et al. (2014) found smaller decreases close to the coast and Mori et al. (2010) found increases in the Bay of Biscay. Fig. 7 shows changes in T_{02} in the North Atlantic with a spatial resolution of 0.5°. Changes in mean period are consistent with changes in wave height. There is a clear decrease in T_{02} except in some northern coastal areas. Maximum decreases of 0.1 s are found for RCP8.5 in the long-term. Decreases in the mean period found by Hemer et al. (2013b) are larger (>0.2 s) and extended farther north and south.

Although significant wave height and mean period are the most commonly used parameters to describe wave climate variability, the method can also be applied to estimate changes in aggregated variables (e.g. wave energy flux). Fig. 8 shows changes in the mean wave energy flux along the European coasts on a grid of 0.125°. A clear decrease in mean wave energy can be seen in both the North Atlantic sub-basin and in the Mediterranean Sea. Changes in the Mediterranean are lower in magnitude than in the Atlantic, but they are relatively large. As expected, larger decreases can be found for RCP8.5 in the long-term. Wave energy flux is proportional to $H_s{}^2 \times T_{02}$, thus, changes with the same sign in both H_s and T_{02} boost much more the wave energy flux. The inter-model variability for H_s, T_{02} and wave energy flux is larger for RCP4.5 and RCP8.5 than for RCP2.6, especially in the northern areas.

5. Summary and conclusions

A regional statistical downscaling of atmospheric conditions to multivariate wave climate has been developed and applied in the North Atlantic sub-basin and the Mediterranean Sea. The method is based on a weather types approach. It allows easy visualization of weather types and associated wave climate. The main advantages of this method are its low computational cost and simplicity. The easy implementation for ensembles allows multi-model analysis for several future climate scenarios. The method allows the detection of the synoptic atmospheric conditions that are expected to be more or less frequent in the future. Future changes in the predictor responsible for changes in the wave climate can also be analyzed. Results show a general decrease in mean wave heights and periods in the North Atlantic and the Mediterranean. The decreases, found for all the analyzed scenarios, are larger for the long-term and high-emissions scenarios. Our results agree with other studies based on large ensembles, both statistical (e.g. Wang et al., 2014) and dynamical (e.g. Hemer et al., 2013b) downscaling. Some differences can be found between this study and other studies based in only one GCM. For example, Mori et al. (2010) found increases in the mean wave height in the Bay of Biscay. The reduction in both significant wave height and wave period produces a clear decrease in mean wave energy in the European coasts. This reduction can affect the profitability of wave energy extraction projects. Further work aims to scale-up this methodology to obtain high-resolution multi-model wave projections globally.

Acknowledgments

The work was partly funded by the FP7 European project CoCoNet (287844). FJM acknowledges the support of the Spanish Ministerio de Economía y Competitvidad under grant BIA2014-59643-R. The authors would like to acknowledge the climate modeling groups which have generated the data used in this study, as well as the PCMDI for facilitating access to it. Finaly, we thank Christine Hegermiller, Sean Vitousek and three anonymous reviewers for the useful comments on an early draft of this manuscript.

References

Amante, C., Eakins, B.W., 2009. ETOPO1 1 arc-minute global relief model: procedures, data sources and analysis. NOAA Technical Memorandum NESDIS NGDC-24. National Geophysical Data Center, NOAA. doi:10.7289/V5C8276M.

Ardhuin, F., Rogers, E., Babanin, A.V., Filipot, J.-F., Magne, R., Roland, A., Van der Westhuysen, A., Queffeulou, P., Lefevre, J.-M., Aouf, L., Collard, F., 2010. Semiempirical dissipation source functions for ocean waves. Part I: definition, calibration, and validation. J. Phys. Oceanogr. 40 (9), 1917–1941. doi:10.1175/2010JPO4324.1.

Camus, P., Menéndez, M., Méndez, F.J., Izaguirre, C., Espejo, A., Cánovas, V., Pérez, J., Rueda, A., Losada, I.J., Medina, R., 2014a. A weather-type statistical downscaling framework for ocean wave climate. J. Geophys. Res.: Oceans. 119 (11), 7389–7405. doi:10.1002/2014JC010141.

Camus, P., Méndez, F.J., Losada, I.J., Menéndez, M., Espejo, A., Pérez, J., Rueda, A., Guanche, Y., 2014b. A method for finding the optimal predictor indices for local wave climate conditions. Ocean Dyn. 64 (7), 1025–1038. doi:10.1007/s10236-014-0737-2.

Chawla, A., Tolman, H.L., 2008. Obstruction grids for spectral wave models. Ocean Modell. 22 (1–2), 12–25. doi:10.1016/j.ocemod.2008.01.003.

Erikson, L.H., Hegermiller, C.A., Barnard, P.L., Ruggiero, P., van Ormondt, M., 2015. Projected wave conditions in the Eastern North Pacific under the influence of two CMIP5 climate scenarios. submitted to Ocean Modelling.

Gleckler, P.J., Taylor, K.E., Doutriaux, C., 2008. Performance metrics for climate models. J. Geophys. Res.: Atmos. 113 (D6), 1984–2012.

Hemer, M.A., Katzfey, J., Trenham, C.E., 2013. Global dynamical projections of surface ocean wave climate for a future high greenhouse gas emission scenario. Ocean Modell. 70, 221–245. doi:10.1016/j.ocemod.2012.09.008.

Hemer, M.A., Fan, Y., Mori, N., Semedo, A., Wang, X.L., 2013. Projected changes in wave climate from a multi-model ensemble. Nat. Clim. Chang. 3 (5), 471–476. doi:10.1038/nclimate1791.

Lamb, H.H., 1972. British Isles weather types and a register of the daily sequence of circulation patterns 1861–1971. Geophysics Memoires. HMSO, London, p. 116.

Laugel, A., Menendez, M., Benoit, M., Mattarolo, G., Méndez, F., 2014. Wave climate projections along the French coastline: dynamical versus statistical downscaling methods. Ocean Modell. 84, 35–50. doi:10.1016/j.ocemod.2014.09.002.

Menéndez, M., Méndez, F.J., Losada, I.J., Graham, N.E., 2008. Variability of extreme wave heights in the northeast Pacific Ocean based on buoy measurements. Geophys. Res. Lett. 35 (22). doi:10.1029/2008GL035394.

Mori, N., Yasuda, T., Mase, H., Tom, T., Oku, Y., 2010. Projection of extreme wave climate change under global warming. Hydrol. Res. Lett. 4, 15–19. doi:10.3178/HRL.4.15.

Moss, R.H., Edmonds, J.A., Hibbard, K.A., Manning, M.R., Rose, S.K., van Vuuren, D.P., et al., 2010. The next generation of scenarios for climate change research and assessment. Nature 463 (7282), 747–756. doi:10.1038/nature08823.

Pérez, J., Menéndez, M., Méndez, F.J., Losada, I.J., 2014a. Evaluating the performance of CMIP3 and CMIP5 global climate models over the north-east Atlantic region. Clim. Dyn. 43 (9–10), 2663–2680. doi:10.1007/s00382-014-2078-8.

Pérez, J., Méndez, F.J., Menéndez, M., Losada, I.J., 2014b. ESTELA: a method for evaluating the source and travel time of the wave energy reaching a local area. Ocean Dyn. 64 (8), 1181–1191. doi:10.1007/s10236-014-0740-7.

Priesendorfer, R.W., 1988. Principal Components Analysis in Meteorology and Oceanography. Elsevier, p. 425.

Rascle, N., Ardhuin, F., 2013. A global wave parameter database for geophysical applications. Part 2. Model validation with improved source term parameterization. Ocean Modell. 70, 174–188. doi:10.1016/j.ocemod.2012.12.001.

Saha, S., Moorthi, S., Pan, H.-L., Wu, X., Wang, J., Nadiga, S., Tripp, P., Kistler, R., Woollen, J., Behringer, D., Liu, H., Stokes, D., Grumbine, R., Gayno, G., Wang, J., Hou, Y.-T., Chuang, H.-Y., Juang, H.-M.H., Sela, J., Iredell, M., Treadon, R., Kleist, D., Van Delst, P., Keyser, D., Derber, J., Ek, M., Meng, J., Wei, H., Yang, R., Lord, S., Van Den Dool, H., Kumar, A., Wang, W., Long, C., Chelliah, M., Xue, Y., Huang, B., Schemm, J.-K., Ebisuzaki, W., Lin, R., Xie, P., Chen, M., Zhou, S., Higgins, W., Zou, C.-Z., Liu, Q., Chen, Y., Han, Y., Cucurull, L., Reynolds, R.W., Rutledge, G., Goldberg, M., 2010. The NCEP climate forecast system reanalysis. Bull. Am. Meteorol. Soc. 91 (8), 1015–1057. doi:10.1175/2010BAMS3001.1.

Saha, S., Moorthi, S., Wu, X., Wang, J., Nadiga, S., Tripp, P., Behringer, D., Hou, Yu.-T., Chuang, H.-ya, Iredell, M., Ek, M., Meng, J., Yang, R., Mendez, M.P., van den Dool, H., Zhang, Q., Wang, W., Chen, M., Becker, E., 2014. The NCEP climate forecast system version 2. J. Clim. 27 (6), 2185–2208. doi:10.1175/JCLI-D-12-00823.1.

Semedo, A., Weisse, R., Behrens, A., Sterl, A., Bengtsson, L., Günther, H., 2013. Projection of global wave climate change toward the end of the twenty-first century. J. Clim. 26 (21), 8269–8288. doi:10.1175/JCLI-D-12-00658.1.

Snodgrass, F.E., Groves, G.W., Hasselmann, K.F., Miller, G.R., Munk, W.H., Powers, W.H., 1966. Propagation of ocean swell across the Pacific. Philos. Trans. R. Soc. A Math. Phys. Eng. Sci. 259 (1103), 431–497. doi:10.1098/rsta.1966.0022.

Tolman, H.L., 2014. User manual and system documentation of WAVEWATCH III version 4.18. NOAA/NWS /NCEP/MMAB Technical Note 316, pp. 194 + Appendices (pdf).

Van Vuuren, D.P., Edmonds, J., Kainuma, M., Riahi, K., Thomson, A., Hibbard, K., Hurtt, G.C., Kram, T., Krey, V., Lamarque, J.-F., Masui, T., Meinshausen, M., Nakicenovic, N., Smith, S.J., Rose, S.K., 2011. The representative concentration pathways: an overview. Clim. Chang. 109 (1–2), 5–31. doi:10.1007/s10584-011-0148-z.

Wessel, P., Smith, W., 1996. A global, self-consistent, hierarchical, high-resolution shoreline database. J. Geophys. Res. 101 (B4), 8741–8743. doi:10.1029/96JB00104.

Wang, X.L., Swail, V.R., Cox, A., 2010. Dynamical versus statistical downscaling methods for ocean wave heights. Int. J. Climatol. 30, 317–332. doi:10.1002/joc.1899.

Wang, X.L., Feng, Y., Swail, V.R., 2014. Changes in global ocean wave heights as projected using multimodel CMIP5 simulations, 1026–1034. doi:10.1002/2013GL058650.1.

Please cite this article as: J. Perez et al., Statistical multi-model climate projections of surface ocean waves in Europe, Ocean Modelling (2015), http://dx.doi.org/10.1016/j.ocemod.2015.06.001